Modulation of thermal and thermoelectric transport in individual carbon nanotubes by fullerene encapsulation

Takashi Kodama[1]*, Masato Ohnishi[2], Woosung Park[1], Takuma Shiga[2], Joonsuk Park[3], Takashi Shimada[4], Hisanori Shinohara[5], Junichiro Shiomi[2] and Kenneth E. Goodson[1]*

The potential impact of encapsulated molecules on the thermal properties of individual carbon nanotubes (CNTs) has been an important open question since the first reports of the strong modulation of electrical properties in 2002[1,2]. However, thermal property modulation has not been demonstrated experimentally because of the difficulty of realizing CNT-encapsulated molecules as part of thermal transport microstructures. Here we develop a nanofabrication strategy that enables measurement of the impact of encapsulation on the thermal conductivity (κ) and thermopower (S) of single CNT bundles that encapsulate C_{60}, $Gd@C_{82}$ and $Er_2@C_{82}$. Encapsulation causes 35–55% suppression in κ and approximately 40% enhancement in S compared with the properties of hollow CNTs at room temperature. Measurements of temperature dependence from 40 to 320 K demonstrate a shift of the peak in the κ to lower temperature. The data are consistent with simulations accounting for the interaction between CNTs and encapsulated fullerenes.

Much attention has been given to thermal transport in CNTs because of potential applications including energy conversion[3] and thermal management[4]. A fundamental investigation of both individual CNTs and their bulk form is important for understanding the overall behaviour of these materials for these applications. The modulation of properties of individual CNTs is of particular interest because it may lead to the improvement of material performance and the discovery of new applications. A key feature of CNTs is the nanoscale internal cavity, and recent advances in chemical engineering have enabled the insertion of a variety of materials into the inner space, such as different types of carbon nanomaterial[5], organic molecule[6], atomic wire[7] and nanoparticle[8]. Previous work revealed that fullerene encapsulation can modulate the electrical properties of CNTs[1,2] and this has created an expectation of a significant modulation of the intrinsic κ. However, the impact of encapsulated molecules on the thermal transport properties of individual CNTs has not been measured yet. The most accurate κ measurements along individual nanomaterials require microfabricated platforms incorporated as part of the suspended target sample. However, this preparation step is challenging because of the difficulty of positioning the target sample on the fragile suspended structure, and this experimental difficulty has proved to be an important barrier to the thermal characterization of nanomaterials.

Figure 1a shows a schematic drawing and a scanning electron microscope (SEM) image of the measurement structure used in this study. Previous κ and S measurements have used a suspended geometry[9–12]. The major innovation in our nanofabrication process is linked to the fact that successful sample preparation has previously relied on a single nanomaterial being situated properly relative to the measurement scaffold in past measurements of thermal properties. This inherently stochastic process made it seem nearly impossible to measure many samples for statistics, which is needed to most rigorously evaluate the κ of nanomaterials. We alleviate this situation in the present work through the use of the periodic nanogrid (PN) structure, which includes a vertically embedded sacrificial oxide layer, as a starting scaffold for the fabrication of the κ and S measurement device. The periodic structure increases the locations at which a sample can be successfully measured. As shown in Fig. 1b, samples are spin-coated over the PN structure, and multistep electron beam (e-beam) lithography is performed on the target samples for the fabrication of the suspended device structure. The target samples are suspended first between the PN oxide and hydrogen silsesquioxane (HSQ) e-beam resist, and the process is completed by the removal of e-beam resists and nanogrid oxide with vapour HF etching. Details are described in the Methods and Supplementary Information. Single-walled carbon nanotubes (SWNTs), double-walled carbon nanotubes (DWNTs), and three kinds of SWNT that encapsulate C_{60}, $Gd@C_{82}$ and $Er_2@C_{82}$ fullerenes (C_{60}, $Gd@C_{82}$ and $Er_2@C_{82}$ peapod, respectively) were synthesized and purified individually by a technique we reported previously (the transmission electron microscopy (TEM) images are shown in Fig. 1b)[13]. The sample damage caused by the fabrication processes has been investigated by Raman spectroscopy and the fabrication procedure developed in this paper is tailored to avoid damage (see Supplementary Information).

Using this methodology, we fabricate suspended κ measurement devices incorporating single bundles of SWNTs ($N = 7$, where N is the number of devices), DWNTs ($N = 4$), C_{60} ($N = 6$), $Gd@C_{82}$ ($N = 2$) and $Er_2@C_{82}$ peapods ($N = 4$), and the κ and S measurements are carried out at room temperature ($T = 300$ K). Figure 2 shows the distribution of the measured κ and S as a function of the diameter and Table 1 summarizes both the average values and the uncertainties. The measurement errors caused by the measurement sensitivity, heat losses, and the thermal contact resistance are

[1]Department of Mechanical Engineering, Stanford University, Stanford, California 94305, USA. [2]Department of Mechanical Engineering, School of Engineering, The University of Tokyo, Tokyo 113-8656, Japan. [3]Department of Materials Science and Engineering, Stanford University, Stanford, California 94305, USA. [4]Institute of Engineering Innovation, School of Engineering, The University of Tokyo, Tokyo 113-8656, Japan. [5]Department of Chemistry, Nagoya University, Nagoya 464-8602, Japan. *e-mail: kodama@photon.t.u-tokyo.ac.jp; goodson@stanford.edu
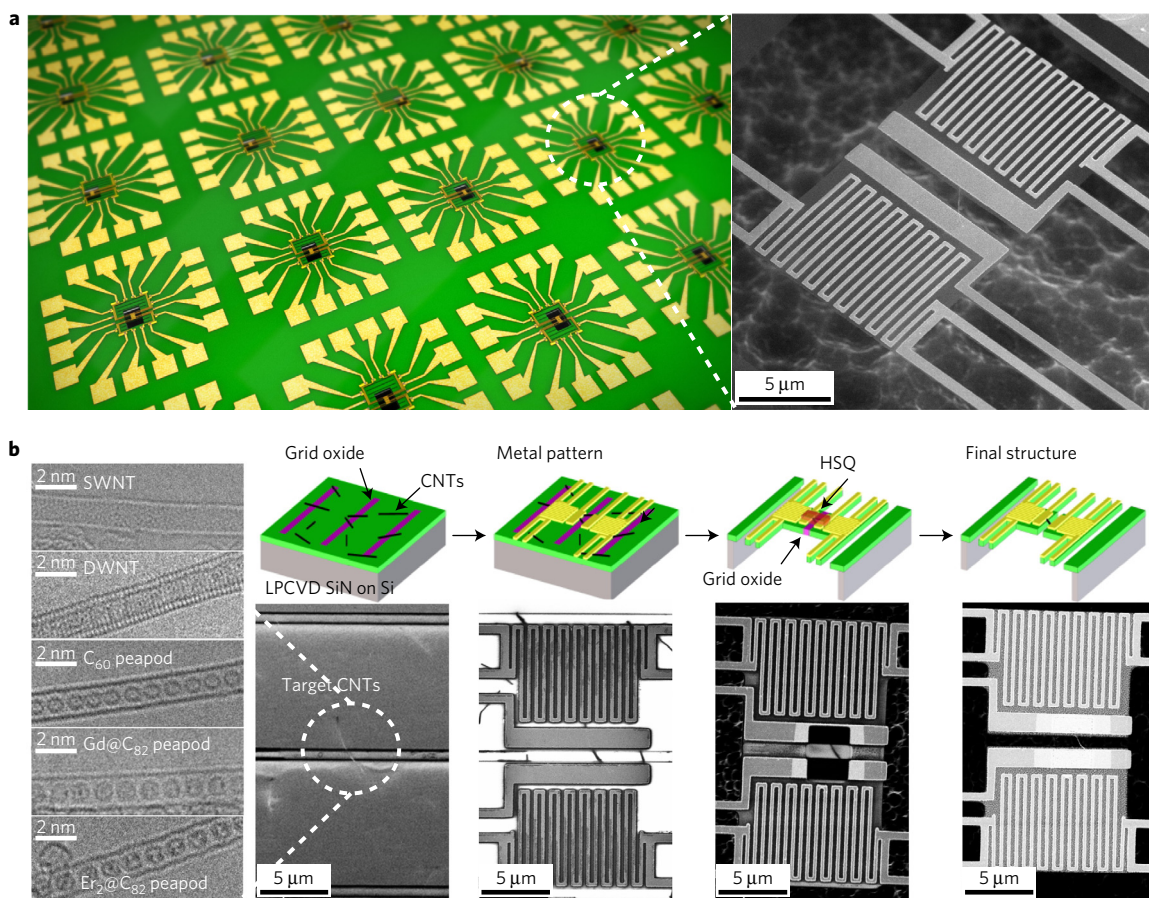
Figure 1 | Schematics, SEM and TEM images of measurement devices and encapsulated CNTs. a, A schematic drawing of manufactured measurement devices (left) and a representative SEM image of the suspended microstructure used for measuring the thermal conductivity (κ) and thermopower of CNTs (right). **b**, Schematic process flow of the fabrication process developed here for the suspended κ measurement device with snapshot SEM images. Details of the fabrication procedure are shown in the Methods and Supplementary Information. On the left are TEM images of the five types of CNT used in this study.

Table 1 | Summary of measured mean values, number of device (N), and the measurement uncertainties of the mean.

	SWNT	DWNT	C_{60} peapod	Gd@C_{82} peapod	Er$_2$@C_{82} peapod
Average thermal conductivity (κ_{ave}), W m^{-1} K^{-1}	200.2 ($\pm$6.5) (N=7)	134.4 ($\pm$14.1) (N=4)	85.4 ($\pm$4.9) (N=6)	126.3 ($\pm$22.8) (N=2)	97.0 ($\pm$17.0) (N=4)
Average thermopower (S_{ave}), μV K^{-1}	27.8 ($\pm$2.2) (N=5)	40.1 ($\pm$2.3) (N=4)	38.9 ($\pm$2.8) (N=6)	32.1 ($\pm$10.5) (N=2)	40.7 ($\pm$2.7) (N=4)
Average electrical conductivity (σ_{ave}), $\times 10^5$ S m^{-1}	1.75 ($\pm$0.32) (N=7)	1.92 ($\pm$0.20) (N=13)	1.47 ($\pm$0.37) (N=3)	1.86 ($\pm$0.34) (N=7)	1.65 ($\pm$0.42) (N=3)

discussed in the Supplementary Information, and the measured values of κ include 5.5–6.5% uncertainties at $T = 300$ K. The measured thermal conductance of single CNT bundles ranges from 10^{-9} to 10^{-8} W K^{-1}. The bundles were defined as a filled cylinder and the volume, V, was calculated by $V = lA = \pi d^2 l / 4$, where A, d and l are the cross-sectional area, the diameter measured by atomic force microscopy, and the length estimated from SEM images, respectively. Figure 2a and Table 1 show that the average κ (κ_{ave}) of an individual SWNT is 200.2 W m^{-1} K^{-1} with small variation while that of 3 kinds of peapod are approximately 35–55% smaller. Furthermore, the average S (S_{ave}) of all of the peapod structures is approximately 40% higher than that of a SWNT without encapsulation (see Fig. 2b

and Table 1). These are all p-type materials. The electrical conductivities (σ) of the suspended samples are measured using separately fabricated 4-probe measurement devices at $T = 300$ K. There is approximately 20% variation in the average σ (σ_{ave}) values for all samples and there is no systematic difference between SWNTs and peapods (see Table 1 and Supplementary Information). Based on the measured values at $T = 300$ K, the thermoelectric figure of merit, ZT ($= \sigma_{ave} S_{ave}^2 T \kappa_{ave}^{-1}$), can be roughly calculated to be 2.03×10^{-4}, 7.81×10^{-4}, 4.55×10^{-4} and 8.45×10^{-4} for SWNTs, C_{60}, Gd@C_{82} and Er$_2$@C_{82} peapods, respectively. The ZT of peapods is observed to be 2–4 times higher than that of SWNTs due to the suppression of κ and the enhancement of S.
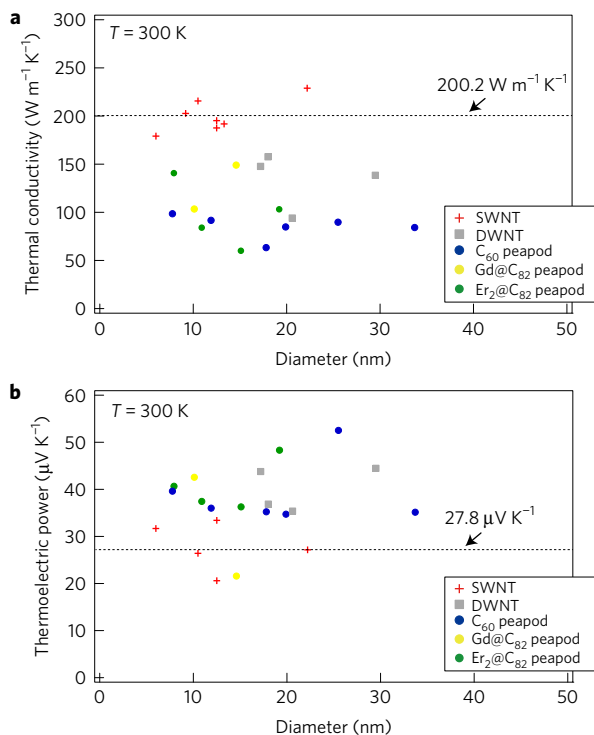
Figure 2 | Thermal conductivity (κ) and thermoelectric power (S) of encapsulated CNT bundles measured at room temperature ($T = 300$ K). a,b, κ (**a**) and S (**b**) of encapsulated CNT bundles as a function of the diameter. The dashed lines show the average κ and S of SWNTs estimated between different samples. All points indicate the experimental results obtained with the individual measurement device, and the respective device information is summarized in Supplementary Figs 5–10. All points in **a** have 5.5–6.5% measurement uncertainties.

Figure 3 | Temperature dependence of the thermal conductivity (κ) and thermoelectric power (S) of encapsulated CNT bundles. a,b, Temperature dependence of κ (**a**) and S (**b**) of encapsulated CNT bundles, respectively. The vertical axis in **a** and **b** shows the κ and S divided by the measurement value at $T = 300$ K, respectively. The results are obtained with the device 'SW4', 'DW2', 'PA1', 'PB1' and 'PC1' shown in Supplementary Figs 5–10.

Figure 3 shows the temperature dependence of κ and S for each sample, respectively. The κ of the SWNT sample increases monotonically and past studies reported that the κ peak of SWNT occurs from $T = 300$–340 K (refs 10–12). The data demonstrate that the κ peak for peapods shifts to lower temperatures ($T = 250$–300 K for C_{60}, and $T = 200$–250 K for metal@C_{82} peapods). The variation depends on the size of the encapsulated fullerenes (diameters of the C_{60} and C_{82} are 7.06 and 8.20 Å, respectively[14,15]), and DWNTs also show similar temperature dependence of κ to C_{60} peapods. There are no remarkable differences among the five different samples in the measured values of the temperature-dependent S, and all exhibit a linear temperature dependence as in previous reports[9–11].

The κ of individual SWNTs and multi-walled carbon nanotubes (MWNTs) have been determined experimentally[9–12,16–20], and the reported values range from 100 to 3,000 W m^{-1} K^{-1} at $T = 300$ K. Previous works have reported that κ of these bundles becomes smaller due to the quenching of some low-frequency phonon modes in the CNTs, which is caused by the physical contact, and small thermal conductance at inter-tube junctions[11,12,19–21]. As the present measurement distance is shorter than the length of individual SWNTs (>1 μm), the low κ primarily originates from the quenching effect. Note that the definition of the cross-sectional area also impacts the spread in the reported κ values. The S values of SWNT (ref. 10) and MWNT (ref. 9) samples have been reported to be approximately 40 and 80 μV K^{-1} at $T = 300$ K, respectively, and the MWNT samples show higher values compared with those of the SWNT. These prior findings are consistent with the present experimental results for SWNT and DWNT bundles.

There have been some theoretical simulations predicting that C_{60} encapsulation enhances κ owing to motion of the encapsulated fullerenes[22–24], and those simulation results are not consistent with the present experimental findings. In terms of relevant experimental data, only buckypaper has been characterized in bulk form for C_{60} peapods[25] and the thermal transport properties of individual peapods are still unknown. For the explanation of the disagreement between predictions and present experimental data, we focus on the interaction between the SWNT and the encapsulated fullerenes. While past theoretical work indicated that C_{60} encapsulation does not cause structural deformation of a SWNT when the diameter of the SWNT is >1.3 nm (refs 22–24,26), past optical[27,28] and atomic force microscopy measurements[29] revealed the radial expansion of the SWNTs. Furthermore, in the present work, we confirm using TEM that the average diameter of peapods is larger than that of hollow SWNTs by about 2–3% (see Supplementary Information). Therefore, we should reconsider the SWNT–C_{60} interaction so as to realize a radial expansion of SWNT. For our theoretical work in this paper we adopt a model system (Model A) featuring a (10, 10) SWNT that encapsulates a closely packed C_{60} molecule (see Fig. 4a). We include van der Waals interactions between the outer (10, 10) SWNT and C_{60} that are modulated by variation of the characteristic distance, σ_{int}, in the Lennard-Jones potential (detailed methodology is described in the Supplementary Information). We define the distance between the SWNT and C_{60} as $\alpha_{int} = d_{int}/d_{max}$ ($d_{int} = (d_{max} - d_f)/2$), where d_{max} and d_f are the diameter of the strained SWNT and the fullerene, respectively (see Fig. 4a). The value of α_{int} becomes larger as σ_{int} increases due to the slight expansion of the SWNT and compression of C_{60}. Figure 4a shows the calculated κ of peapods as a function of α_{int} at $T = 300$ K. The value of κ decreases dramatically by about 50% with the slight radial expansion of the
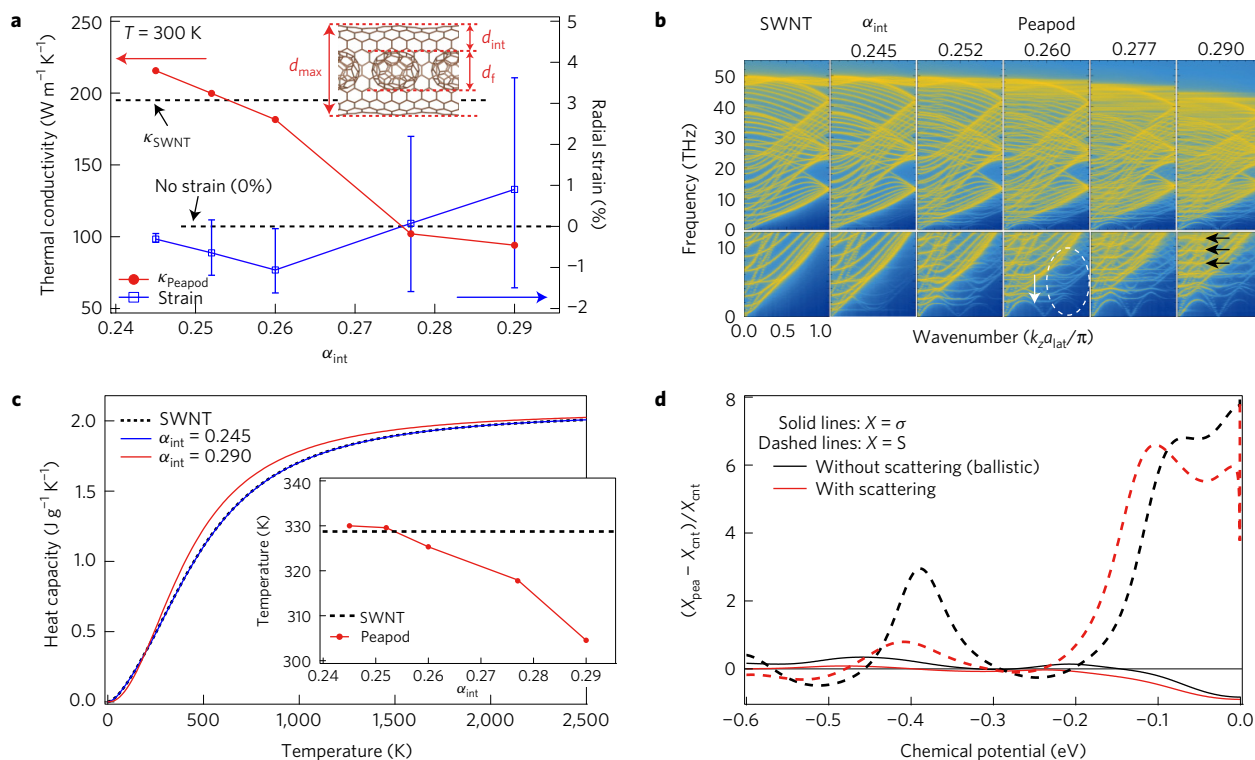
Figure 4 | Simulations of SWNT samples with encapsulation. a, Thermal conductivity (κ) of the C_{60} peapod at $T = 300$ K as a function of $\alpha_{int} (= d_{int}/d_{max}$, where $d_{int} = (d_{max} - d_f)/2$). The left and right vertical axes show the κ and the average radial strain of the outer (10, 10) SWNT, respectively. The higher and lower error bars of the strain correspond to the maximum and minimum values, respectively. The κ of the empty (10, 10) SWNT and 0% strain are indicated with black dashed lines. The inset schematic shows the present simulation model (Model A) for the C_{60} @ (10, 10) SWNT. **b**, Phonon dispersion relations of the C_{60} peapod with variation of α_{int}. The vertical and horizontal axes show the phonon frequency and wavenumber normalized by the Brillouin boundary length, $k_z a_{lat}/\pi$, where k_z and a_{lat} are a wavevector and lattice constant, respectively. **c**, Heat capacity of the C_{60} peapod as a function of α_{int} and temperature. The inset data show the temperature at which the heat capacity becomes 0.7 J g^{-1} K^{-1} as a function of α_{int}. **d**, The change ratio, $(X_{cnt} - X_{pea})/X_{cnt}$, of $X = \sigma$ (solid line) and $X = S$ (dashed line) caused by fullerene encapsulation as a function of the chemical potential. The red and black lines correspond to the calculation results with electron scattering and without scattering (fully ballistic), respectively.

SWNT when $\alpha_{int} > 0.272 \pm 0.013$ (experimental value estimated by present TEM measurements of C_{60} peapods, $N = 21$), and the reduction of the predicted κ and the expansion of the SWNT both agree well with the experimental results. Therefore, it is suggested that the disagreement with past theoretical work may originate from an underestimation of repulsion between the SWNT and C_{60}, and that the resulting larger deformations may cause the reduction of κ.

We use the calculations developed here to predict the phonon properties to understand the mechanism responsible for the reduction of κ and the shift in the peak of the measured temperature-dependent κ associated with the encapsulation. As shown in Fig. 4b, the high-frequency phonon modes whose eigenvectors are displaced along the axial and azimuthal directions are softened with increasing α_{int}. The softening occurs because the local radial strain weakens the bonding between the carbon atoms and shifts the heat capacity (c_{lat}) profile to lower temperature (see Fig. 4c). The inset of Fig. 4c shows the temperature at which the c_{lat} becomes 0.7 J g^{-1} K^{-1} and the data show the shift of the c_{lat} profile to lower temperature by about 20 K when $\alpha_{int} = 0.29$. While the shift is consistent with the present experimental results, the temperature shift is smaller than the observed peak shift of κ (50–100 K) and the c_{lat} profile solely does not explain the experimental results quantitatively.

Thus, to further deepen the discussion, we develop a second set of simulations using a model (Model B) that targets more uniform radial strain. Specifically, we use a (5, 5) SWNT@(10, 10) system to provide a uniform radial strain to the outer (10, 10) SWNT, and study the effect of radial-strain distribution on heat conduction

in the longitudinal direction (see Supplementary Information and Supplementary Fig. 3). The simulations from Model B also show suppression of κ, softening of high-frequency phonons, and a shift of the c_{lat} profile to lower temperature as the uniform radial stain increases. However, an unusually large radial strain ($>12.5\%$) is required to realize the large variation of the properties in the model, and the difference in the results between Models A and B indicates the presence of unique effects caused by the wavy deformation due to encapsulated fullerenes.

Figure 4b shows that, in Model A, the wavy deformation of the outer SWNT generates new phonon bands due to zone-folding effects. Since fullerenes are placed in SWNTs with the interval of approximately four primitive unit cells of SWNTs, the new bands appear with the periodicity of $\pi/(2a_{lat})$, which is a fourth of the Brillouin zone length (for example, indicated by the white arrow and dashed circle in Fig. 4b). Furthermore, the interaction between the SWNT and fullerenes flattens the phonon bands of the SWNT (indicated by black arrows in Fig. 4b) in the wide range of frequency, originated from the mode-hybridization with the vibration of fullerenes. These modulations in the SWNT phonon bands are absent in Model B, and, thus, are due to the non-uniform interaction with the local fullerenes. The band flattening (which can be viewed as phonon localization) decreases the group velocities and thus the thermal conductivity. In addition, the reduction of Brillouin zone and the softening of phonon bands increase the scattering phase space of Umklapp scattering. If we see the peak in temperature dependence of κ as a result of competition of c_{lat} and phonon relaxation time that increases and decreases with

temperature, respectively, the enhanced Umklapp scattering rate (inverse relaxation time) should also contribute to the peak shift. In summary, the simulations using Models A and B indicate that the suppression of the κ observed experimentally in this paper originates from the non-uniform interaction between the SWNT and the encapsulated fullerenes. The shift in the temperature of the peak in κ originates from both the enhancement of Umklapp scattering and the shift of the c_{lat} profile to lower temperature.

The encapsulation effect on the thermoelectric properties has also been investigated by means of the Landauer formalism to gain insight into the measured variation of S and σ (detailed discussion is provided in the Supplementary Information). As the Seebeck coefficient depends on the chirality of SWNT samples, we perform the simulation on various types of (n, m) SWNT whose diameters are in the range of 1.2–1.5 nm. The results show that the radial strain enhances S when the classification index, $p\ (=|n-m|-3q$, where q is an integer), is -1 or 0 and reduces S otherwise (that is, $p=+1$). In particular, the metal-to-semiconducting transition significantly increases S of the CNT bundles. We perform additional simulations with further realistic model systems that account for electron scattering (see Supplementary Information in detail). As shown in Fig. 4d, the fullerene encapsulation remarkably enhances the S of CNT bundles while it does not have a large impact on σ over a wide range of the chemical potential regardless of the strength of electron scattering, which are consistent with the experimental findings. Therefore, the observed variations in the thermoelectric properties may be reasonably attributed to the radial expansion of SWNTs caused by fullerene encapsulation.

A suppression of κ and an enhancement of S are reported here for CNTs that encapsulate fullerene molecules, and we conclude that this variation is caused by the strong interaction between CNTs and the encapsulated materials. These results indicate the possible further modulation of the thermal properties of CNTs by variation of the encapsulated molecules. Many applications of CNTs require the bulk form, and in the case of CNT-based thermoelectric materials, the thermal transport through inter-tube junctions of CNTs usually exerts a large impact on the overall thermal conduction properties[3]. However, the conduction properties of individual CNTs will impact the bulk material properties in the case that the morphology of CNT networks is optimized for orientation and density of CNTs[30]. The structural optimization is necessary to further improve the material performance because the random orientation leads to the reduction of the σ and limits the density of CNTs in the film. Furthermore, the present experimental findings regarding the enhancement of S are expected to improve the material performance because S of inter-tube junctions is primarily determined by the S of individual CNTs. Therefore, we believe that modulation of the thermoelectric properties of individual CNTs will also be important for applications.

Methods

Methods, including statements of data availability and any associated accession codes and references, are available in the online version of this paper.

References

1. Hornbaker, D. J. et al. Mapping the one-dimensional electronic states of nanotube peapod structures. *Science* **295,** 828–831 (2002).
2. Lee, J. et al. Bandgap modulation of carbon nanotubes by encapsulated metallofullerenes. *Nature* **415,** 1005–1008 (2002).
3. Avery, A. D. et al. Tailored semiconducting carbon nanotube networks with enhanced thermoelectric properties. *Nat. Energy* **1,** 16033 (2016).
4. Panzer, M. A. et al. Temperature-dependent phonon conduction and nanotube engagement in metalized single wall carbon nanotube films. *Nano Lett.* **10,** 2395–2400 (2010).
5. Smith, B. W., Monthioux, M. & Luzzi, D. E. Encapsulated C_{60} in carbon nanotubes. *Nature* **396,** 323–324 (1998).
6. Zhang, J. et al. Synthesis and transformation of linear adamantane assemblies inside carbon nanotubes. *ACS Nano* **6,** 8674–8683 (2012).
7. Kitaura, R., Imazu, N., Kobayashi, K. & Shinohara, H. Fabrication of metal nanowires in carbon nanotubes via versatile nano-template reaction. *Nano Lett.* **8,** 693–699 (2008).
8. Liu, X. et al. Design of covalently functionalized carbon nanotubes filled with metal oxide nanoparticles for imaging, therapy, and magnetic manipulation. *ACS Nano* **8,** 11290–11304 (2014).
9. Kim, P., Shi, L., Majumdar, A. & McEuen, P. L. Thermal transport measurements of individual multiwalled nanotubes. *Phys. Rev. Lett.* **87,** 215502 (2001).
10. Yu, C., Shi, L., Yao, Z., Li, D. & Majumdar, A. Thermal conductance and thermopower of an individual single-wall carbon nanotube. *Nano Lett.* **5,** 1842–1846 (2005).
11. Shi, L. et al. Measuring thermal and thermoelectric properties of one-dimensional nanostructures using a microfabricated device. *J. Heat Transfer* **125,** 881–888 (2003).
12. Pettes, M. T. & Shi, L. Thermal and structural characterizations of individual single-, double-, and multi-walled carbon nanotubes. *Adv. Funct. Mater.* **19,** 3918–3925 (2009).
13. Shimada, T. et al. Ambipolar field-effect transistor behavior of $Gd@C_{82}$ metallofullerene peapods. *Appl. Phys. Lett.* **81,** 4067–4069 (2002).
14. Kratschmer, W., Lamb, L. D., Fostiropoulos, K. & Huffman, D. R. Solid C_{60}: a new form of carbon. *Nature* **347,** 354–358 (1990).
15. Takata, M. et al. Confirmation by X-ray diffraction of the endohedral nature of the metallofullerene $Y@C_{82}$. *Nature* **377,** 46–49 (1995).
16. Pop, E., Mann, D., Wang, Q., Goodson, K. & Dai, H. Thermal conductance of an individual single-wall carbon nanotube above room temperature. *Nano Lett.* **6,** 96–100 (2006).
17. Fujii, M. et al. Measuring the thermal conductivity of a single carbon nanotube. *Phys. Rev. Lett.* **95,** 065502 (2005).
18. Hone, J., Whitney, M., Piskoti, C. & Zettl, A. Thermal conductivity of single-walled carbon nanotubes. *Phys. Rev. B* **59,** R2514–R2516 (1999).
19. Hsu, I.-K. et al. Optical absorption and thermal transport of individual suspended carbon nanotube bundles. *Nano Lett.* **9,** 590–594 (2009).
20. Aliev, A. E. et al. Thermal conductivity of multi-walled carbon nanotube sheets: radiation losses and quenching of phonon modes. *Nanotechnology* **21,** 035709 (2010).
21. Ong, Z.-Y., Pop, E. & Shiomi, J. Reduction of phonon lifetimes and thermal conductivity of a carbon nanotube on amorphous silica. *Phys. Rev. B* **84,** 165418 (2011).
22. Vavro, J., Llaguno, M. C., Satishkumar, B. C., Luzzi, D. E. & Fischer, J. E. Electrical and thermal properties of C_{60}-filled single-wall carbon nanotubes. *Appl. Phys. Lett.* **80,** 1450–1452 (2002).
23. Noya, E. G., Srivastava, D., Chernozatonskii, L. A. & Menon, M. Thermal conductivity of carbon nanotube peapods. *Phys. Rev. B* **70,** 115416 (2004).
24. Kawamura, T., Kangawa, Y. & Kakimoto, K. Investigation of the thermal conductivity of a fullerene peapod by molecular dynamics simulation. *J. Cryst. Growth* **310,** 2301–2305 (2008).
25. Cui, L., Feng, Y. & Zhang, X. Dependence of thermal conductivity of carbon nanopeapods on filling ratios of fullerene molecules. *J. Phys. Chem. A* **119,** 11226–11232 (2015).
26. Ohno, Y. et al. Synthesis of carbon nanotube peapods directly on Si substrates. *Appl. Phys. Lett.* **86,** 023109 (2005).
27. Okada, S., Saito, S. & Oshiyama, A. Energetics and electronic structures of encapsulated C_{60} in a carbon nanotube. *Phys. Rev. Lett.* **86,** 3835–3838 (2001).
28. Okazaki, T. et al. Optical band gap modification of single-walled carbon nanotubes by encapsulated fullerenes. *J. Am. Chem. Soc.* **130,** 4122–4128 (2008).
29. Ashino, M. et al. Atomically resolved mechanical response of individual metallofullerene molecules confined inside carbon nanotubes. *Nat. Nanotech.* **3,** 337–341 (2008).
30. He, X. et al. Wafer-scale monodomain films of spontaneously aligned single-walled carbon nanotubes. *Nat. Nanotech.* **11,** 633–638 (2016).

Acknowledgements

Author contributions

T.K. led the project and contributed to the experimental works including device design, fabrication, and conduction measurement. M.O., T.Shiga and J.S. contributed to the theoretical work. W.P. contributed to the SEM imaging and conduction measurement. J.P. contributed to the TEM imaging. T.Shimada and H.S. synthesized and provided all of the CNT samples used in the project. K.E.G. served both as PI and primary advisor for the thermal and thermoelectric measurements. T.K., M.O., T.Shiga, J.S. and K.E.G. wrote the paper.

Additional information

Supplementary information is available in the online version of the paper. Reprints and permissions information is available online at www.nature.com/reprints. Publisher's note: Springer Nature remains neutral with regard to jurisdictional claims in published maps and institutional affiliations. Correspondence and requests for materials should be addressed to T.K. or K.E.G.

Competing financial interests

The authors declare no competing financial interests.

Methods

Fabrication of periodic nanogrid (PN) structure. First, a Si_xN_y film of thickness between 100 and 200 nm is formed on a standard silicon (100) wafer using low-pressure chemical vapour deposition (LPCVD) and periodic 500–800 nm wide lines are patterned by e-beam lithography after coating with a positive e-beam resist (ZEP-520a e-beam resist, ZEON). Next, the patterned area is etched vertically through the Si_xN_y film to fabricate approximately 500-nm-deep trenches by reactive ion etching, and the e-beam resist is removed with acetone, oxygen plasma, and a piranha solution. Next, approximately 1-μm-thick silicon dioxide is deposited on the top surface by plasma-enhanced chemical vapour deposition (PECVD oxide) and the PECVD oxide is planarized by chemical mechanical polishing such that the over-etching of the LPCVD Si_xN_y film is minimized. Finally, 20-nm-thick platinum lines and contact pads with a 5-nm-thick chromium adhesion layer (Pt/Cr) are patterned by photolithography.

Thermal conductivity measurement scaffold fabrication using the periodic nanogrid (PN) structure. The thermal conductivity measurement scaffold is fabricated by three-step e-beam lithography with the PN structure. First, CNTs are dispersed in 1,2-dichloroethane and the sample is spin-coated on the PN structure. The low-magnification SEM images are taken of the PN structure to find appropriate target CNTs, and their topographic images are taken by atomic force microscopy to estimate the diameter of the target CNTs. Next, nanoscale metal patterns are fabricated by e-beam lithography, e-beam evaporation of 60/5-nm-thick Pt/Cr, and a subsequent lift-off process. As a next step, a hydrogen silsesquioxane (HSQ, Dow Corning) e-beam resist is patterned on the target sample by e-beam lithography. Next, the area of the device to be suspended is patterned on a ZEP-520a e-beam resist by another e-beam lithography step, and a Si_xN_y film in the open area is etched away by reactive ion etching. Next, both the heating and sensing Si_xN_y membranes with supporting metal legs are suspended with the top e-beam resist by an isotropic Si etching with XeF_2 gas. Finally, after removal of the top e-beam resist by oxygen plasma cleaning, the HSQ e-beam resist and nanogrid oxide between the heating and sensing membrane are etched away by a vapour HF process.

Data availability. The data that support the findings of this study are available from the corresponding authors upon reasonable request.